Fuel 333 (2023) 126530

Contents lists available at ScienceDirect

Fuel

journal homepage: www.elsevier.com/locate/fuel

Full Length Article

Experimental and numerical study on flame fusion behavior of premixed hydrogen/methane explosion with two-channel obstacles

Shuo Wang [a], Guoqing Xiao [a,b,*], Hongfu Mi [c,*], Yu Feng [d], Jian Chen [e]

[a] College of Chemistry and Chemical Engineering, Southwest Petroleum University, Chengdu 610500, China
[b] Oil & Gas Fire Protection Key Laboratory of Sichuan Province, Chengdu, Sichuan 611731, China
[c] College of Safety Engineering, Chongqing University of Science and Technology, Chongqing 401331, China
[d] School of Chemical Engineering, Oklahoma State University, Stillwater, OK 74078, USA
[e] Center for Offshore Engineering and Safety Technology, China University of Petroleum (East China), Qingdao 266580, China

ARTICLE INFO

Keywords:
Gas explosion
Flame fusion
Two-channel obstacles
Numerical simulation
Turbulent

ABSTRACT

Methane blending with hydrogen has become an effective method to utilize clean energy, the safety of which has attracted much attention. However, there is still lack of studies on the propagation characteristics of premixed flame in split conditions. Therefore, experimental and numerical studies have been conducted to investigate the explosion flame behavior of hydrogen/methane with two-channel obstacle. The effects of the position and barrier ratio of the two-channel obstacle were analyzed based on nine distinguished explosion experiments with different setups. Experimental results show that the explosion flame will generate split and fusion, during its propagation through the two-channel obstacle. The fusion behavior of the split flame changes with the position and barrier ratio of the obstacle, i.e., either complementary or merging. As the obstacle moving further away from the ignition, the maximum speed increases and then decreases. The maximum speed can be increased by more than 5 times. Additionally, the dominance of the cumulative effect of pressure at increasing leads to the monotonicity of pressure. Finally, the flame propagation process, the mechanism of flame fusion, and the turbulence intensity distribution were predicted and visualized by computational fluid dynamics (CFD) based numerical simulations.

1. Introduction

Sustainable energy development and energy security issues have been the focus of attention [1]. Hydrogen is a versatile energy carrier that can help address various energy challenges[2]. However, hydrogen is costly to produce and transport. To address such a challenge, it has been proposed to add hydrogen (H_2) to methane in a specific ratio to compose a mixture of gas fuel for use [345]. In the transition from conventional natural gas to clean energy (i.e., H_2), the criteria for using clean energy require the coordination of economy, environment, and safety [6]. One that requires special attention is energy safety, which is related to human industrial production and daily life. Therefore, it is necessary to make continuous progress in understanding the hazards of uncontrolled mixture gas fuel explosion.

Gas explosion accidents have always been a hot issue in the industry and daily life [78]. When adding hydrogen to methane, the explosion pressure peak value and the maximum rate of rise gradually increase, which will cause more serious hazards [9]. The propagation characteristics of premixed explosions in simple scenarios are well known [10111213141516]. Deformation and distortion of the flame in obstacle conditions have an important effect on the explosion parameters. Cao et al. [17] found that obstacles can affect flame propagation by changing the flame structure. Zhang et al. [18] demonstrated that reducing the early acceleration time of the flame, and positioning closer to the igniter with smaller obstacles, can reduce the maximum flame propagation speed and overpressure. Li et al. [19] identified that flame acceleration with obstacles could influence the mutual promotion of flame instability and obstacle-induced turbulence. Yang et al. [20] proved that obstacles can enhance flame deformation and oscillation, thus accelerating flame propagation. Zheng et al. [21] indicated that the flame front inversion after an obstacle is a purely hydrodynamic phenomenon. Zhang et al. [22] proved that the shorter the distance between the ignition and the obstacle, the greater the interference effect of the obstacle on the explosion. Li et al. [23] revealed that when the obstacle is located near the

* Corresponding authors at: College of Chemistry and Chemical Engineering, Southwest Petroleum University, Chengdu 610500, China (G. Xiao).
E-mail addresses: xiao13541694312@126.com (G. Xiao), mimihh5@163.com (H. Mi).

https://doi.org/10.1016/j.fuel.2022.126530
Received 8 September 2022; Received in revised form 16 October 2022; Accepted 25 October 2022

center of the pipe, the maximum pressure of the explosion reaches near the open end. Zhou et al. [24] proved that due to the reflection and diffraction of pressure waves, external obstacles could cause a rise in pressure in the vicinity. Wen et al. [25] identified that the farthest configuration of the obstacle generates higher pressure, which takes longer to reach the maximum. Lv et al. [26] discovered that the occurrence of the maximum explosion overpressure depends mainly on the maximum flame surface area in the pipe. Schiavetti et al. [27] found that the effect of repeated obstacles on the increase in maximum pressure is higher than the effect of an increased barrier ratio.

Computational fluid dynamics (CFD) has also been developed in recent years with the improvement of high-performance computing. CFD is an essential method for simulating and analyzing the consequences of premix explosions based on the first principles of physics and chemistry. Henriksen et al. [28] used the CFD method to simulate the complete process of flame propagation of premixed gas explosions. Gao et al. [29] found through simulation that the shape of the flame could easily cause many wrinkles in the tube with obstacles. Gamezo et al. [30] simulated the evolution of premixed flames using two reactive fluid dynamics codes (ALLA and FAST). They found that the increase in barrier ratio promoted flame acceleration. In contrast, the high barrier ratio hindered the development of explosions. The simulation results by Qin and Chen [31] revealed that the difference in barrier ratio caused only a small difference in the degree of flame deformation, but the Rayleigh-Taylor instability accompanied the entire flame propagation process. Di Sarli et al. [32] adopted a simulation approach. They found that a flame crossing an obstacle would roll around the vortex until it eventually consumed the entire vortex.

The existing research effort on gas explosions has focused more on the contribution of single-channel obstacles to explosions [33]. The flame maintains its original boundary structure undamaged throughout the propagation. The vortices and flow instabilities are more dominant at the outer flame boundary [3435]. However, complex conditions such as realistic industrial environments or in practical applications with combustible gas may cause uncontrolled explosion flames to exhibit more diverse morphological variations [3637], thus changing the flame dynamics characteristics and intensity [38]. What can make the flame propagation pattern change is not only the number of obstacles, but also the obstacle channel arrangement, which is more important. Increased flame paths caused by parallel alignment of obstacles can change the action behavior of large and small vortices on the flame. The more disordered flame morphology also reflects the degree of chaos in the flame region. The instability features involved in the outer flame boundary may change the flame propagation behavior and explosion hazard level more directly. These factors must be considered when there is a risk of premixed gas explosions in complex conditions.

To complement the study of explosion flame details and pressure development patterns in more than one channel obstacle, this paper conducts a synergistic study using both experiment and numerical simulations of two-channel obstacles on the explosion of premixed hydrogen/methane gas. Specifically, advantages and disadvantages of flame propagation were analyzed by quantifying the split-fusion behavior of flame. Furthermore, the variation of maximum flame propagation speed and overpressure with barrier ratio and obstacle position were also determined. Finally, the CFD simulations were performed to find the reasons and mechanisms of the special flame propagation pattern.

2. Experimental and numerical simulation setup

2.1. Experimental devices

The explosion experiments were performed at an independent experimental platform. Schematic of the experimental setup with device connections is shown in Fig. 1. It includes a gas transport and storage system, an electric spark ignition system, and explosion parameters testing system. The 20 % of hydrogen in the mixture fuel is the most common ratio today, and this ratio of hydrogen has been certified safe for use in existing equipment [394041]. Therefore, the volume fraction of hydrogen in this work was 20 %. The calculated as $\varphi = V_{H_2}/(V_{H_2} + V_{CH_4})$, and the equivalence ratio of the fuel is 1.0. Hydrogen and methane were pre-stored in cylinders with 99.99 % purity. Air was pre-stored in compressor. The ALICAT 20 gas mass flowmeters mixed the three gases and conveyed them into the 600 mm × 80 mm × 80 mm polymethyl methacrylate tube. The ignition is located in the left wall, which consists of two metallic platinum wires that generate an electric spark to trigger the explosion. The flame snapshots were recorded by Phantom VEO 710 high-speed camera, which is connected to a computer and the resolution was 1280 × 280, the sampling frequency was 2000 fps, the exposure time was 490 μs. A pressure sensor manufactured by PCB Piezotronics was installed downstream of the tube. The digital data was converted analog data by the Blast-PRO tester, which the sample rate was 125 kHz.

A total of three two-channel obstacles as shown in Fig. 2. The obstacle arranged in order at 100 mm, 200 mm, 300 mm from the ignition and labeled with Position-1, Position-2, Position-3. The barrier ratio (Br) from small to large are Br = 0.375 (small), Br = 0.5625 (medium), and Br = 0.75 (large).

2.2. Experimental process

Experimental processes are summarized below.

(1) Install and test system shown in Fig. 1.
(2) Check and ensure that all systems are functional and can be used.
(3) Use the plastic film to seal the explosion outlet [4243].

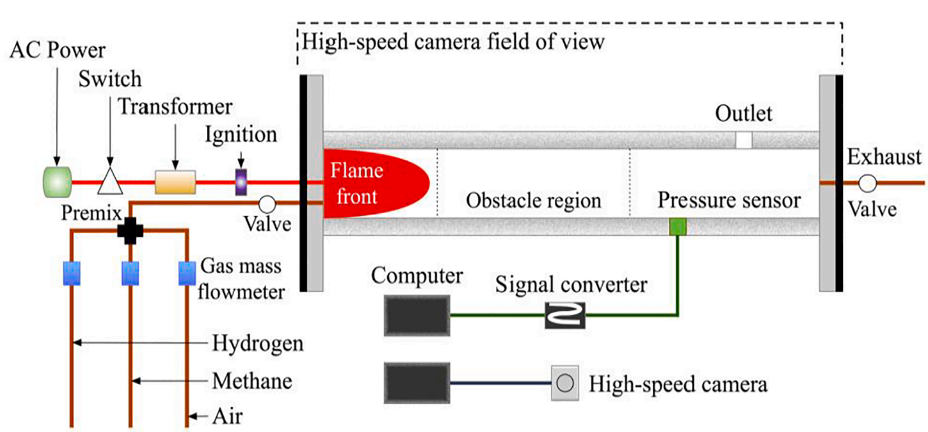

Fig. 1. Schematic diagram of the experimental system.

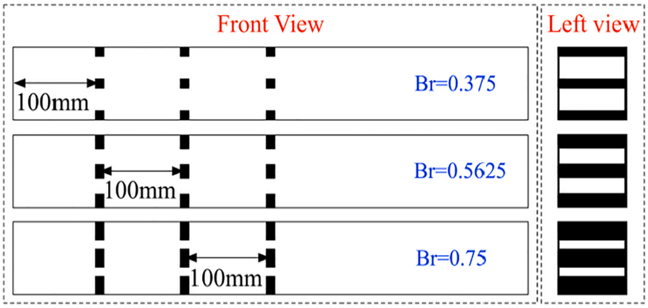

Fig. 2. The position and barrier ratio of the two-channel obstacle.

(4) Close the valve after finishing venting, and stand the gas for 20 s to ensure the repeatability of the experiment [10].
(5) Adjust the high-speed camera and pressure test system to the automatic trigger mode.
(6) Repeat the experiments with multiple trials to avoid experimental serendipity and fluctuations in the test system.

2.3. Numerical simulation setup

A 2D model of 600 mm × 80 mm was adopted to simulate the premixed flame reacting flow and three cases of two-channel obstacles set in Position 1. Zhou et al. [44] demonstrated that small-scale characteristics in the flow can be shown as the maximum size of the mesh is theoretically smaller than the minimum size of any structural feature of the geometry. To match the criterion mentioned above in order to visualize the small-scale flow characteristics, mesh size of 1.0 mm were satisfied and has been validated[453246]. Three-layer adaptive refinement with time based on temperature gradient was also applied (see Fig. 3) to capture the high-gradient regions in the computational domain [474849]. Standard wall functions compatible with RNG k-ε turbulent model [47] were used in the near-wall turbulent boundary layer to make transition to free stream region near the center of the channel. The initial conditions of temperature and pressure are $T_0 = 300$ K, $P_0 = 101{,}325$ Pa.

2.4. Governing equations

The continuity equation, momentum equation, energy equation, material balance equation, and ideal gas law equation were solved are listed below [3150].

$$\frac{\partial \rho}{\partial t}+\frac{\partial}{\partial x_i}(\rho u_i)=0 \tag{1}$$

$$\frac{\partial}{\partial t}(\rho u_i)+\frac{\partial}{\partial x_i}(\rho u_i u_j) = -\frac{\partial P}{\partial x_i}+\frac{\partial \sigma_{ij}}{\partial x_j} \tag{2}$$

$$\frac{\partial}{\partial t}(\rho e)+\frac{\partial}{\partial x_i}(u_i(\rho e+P)) = \frac{\partial}{\partial x_i}\left(k\frac{\partial T}{\partial x_i}-\sum h_m J_m+u_j\sigma_{ij}\right)+\dot{Q}_c \tag{3}$$

$$\frac{\partial}{\partial t}(\rho Y_m)+\frac{\partial}{\partial x_i}(\rho u_i Y_m) = \frac{\partial}{\partial x_i}\left(\rho D_m\frac{\partial Y_m}{\partial x_i}\right)+\dot{\omega}_m \tag{4}$$

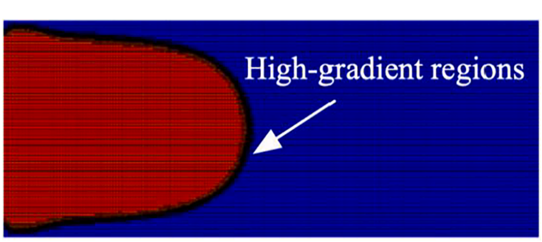

Fig. 3. Adaptive refinement grid.

$$\sigma_{ij} = \mu\left(\frac{\partial u_i}{\partial x_j}+\frac{\partial u_j}{\partial x_i}\right)-\frac{2}{3}\mu\frac{\partial u_i}{\partial x_i}\delta_{ij} \tag{5}$$

$$P = \rho RT \tag{6}$$

where ρ is the density, t is the time, x_i is spatial coordinates in the i direction, u_i is the flow velocity in i direction, σ_{ij} is the stress tensor, P is the pressure, k is the coefficient of heat conduction, $\dot{Q}_c$ is the heat source released by chemical reactions, e is the internal energy as $e = -p/\rho + v_i^2/2$, D_m is the diffusivity coefficient, Y_m is the mass fraction, h_m is the specific enthalpy, $\dot{\omega}_m$ is the reaction rate, and J_m is the diffusion flux of component m. μ is the viscosity, δ_{ij} is the Kronecker delta, R is the gas constant, T is the temperature.

The RNG k-ε turbulent model was more suitable for gas explosion condition [34]. In the RNG k-ε turbulence model, $C_{1\varepsilon}$ was a constant of 1.42 and $C_{2\varepsilon}$ was a constant of 1.68. The Eddy Dissipation Concept (EDC) model was used to couple the turbulence-chemical reaction [51]. The EDC model assumes that chemical reactions occur in a small-scale turbulent structure and the volume ratio C_ξ was 2.1377, the time scale C_τ was 0.4082. The thermal conductivity and dynamic viscosity of each component were calculated separately using the kinetic theory and Sutherland's formula [52]. The convective term discretized by second-order upwind, and the spatial discretization used is in second-order central difference format. The mass, momentum, and energy equation residuals are less than 1×10^{-5}, 1×10^{-5}, and 1×10^{-6}. The numerical simulation adopted Ansys Fluent 2021 code.

3. Experimental results and discussions

3.1. Flame propagation morphology and process

Clanet and Searby [53] proposed four stages of premixed flame propagation corresponding to the time of $t_{sphere} = 10 \pm 2$ ms, $t_{wall} = 26 \pm 2$ ms, and $t_{tulip} = 33 \pm 2$ ms. The propagation of the flame without obstacle is shown in Fig. 4. The time of flame features are $t_{sphere} = 9.5$ ms, $t_{wall} = 24$ ms, and $t_{tulip} = 30$ ms, respectively, satisfying the theoretical data. The accumulation of Rayleigh-Taylor instability (RTI) and pressure waves eventually inverts the flame front, producing the classic tulip flame shape (t = 35 ms). The characteristic behavior of all the above flames maintains one main body.

Fig. 5 illustrates the morphological and propagation process of the premixed flame with two-channel obstacles. The evolution of the flame before contact with the obstacle follows the classic process [53]. However, the flame front splits into two parts by the obstacle when it passes through the two-channel obstacle.

In Fig. 5 (a), the flame involute slightly toward the middle obstacle at t = 15 ms. Both vortex and pressure gradients cause the flame to curl [31], and due to the boundary layer effect, the flame tends to curl more in the direction of the reduced resistance gradient. The boundary of the splitting flame is as wide as the channel at the initial stage of passing through the obstacle. Subsequently, two independent flames expand longitudinally centered on their respective horizontal baselines. It is worth noting that the two parts of the split flame that are close to each other will recombine again at t = 16.5 ms ~ 17.5 ms. The relationship of the flames in the fusion process is not reciprocal, but rather the erosion of one part of the flame to the other. The increased turbulence at the two mutually converging boundaries provides the impetus for flame propagation. At between t = 19.5 ms and t = 23 ms, the flame bodies fuse, but the flame fronts still have two protrusions, which leads to the formation of two tulip structures (between t = 25.5 ms and t = 26.5 ms). Previous studies have shown that RTI is the main cause of tulip flame [34355455]. Obviously, the instability of the flame is increased. The increase in the number of forwarding projections of the flame is conducive to the damage of the limiting of the original boundary layer. Although the main part of the flame fuses into a whole, the flame fronts

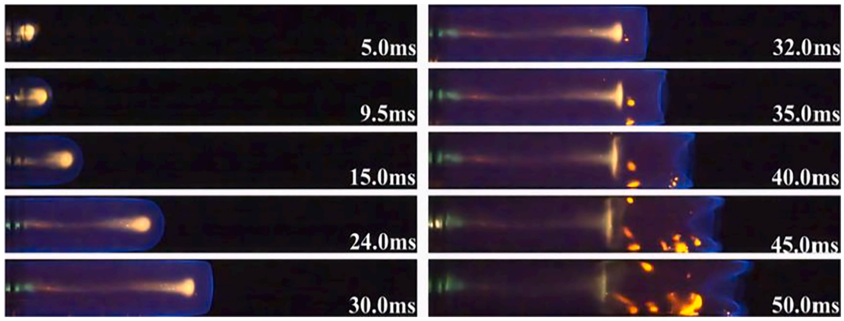

Fig. 4. Premixed hydrogen/methane explosion flame propagation process.

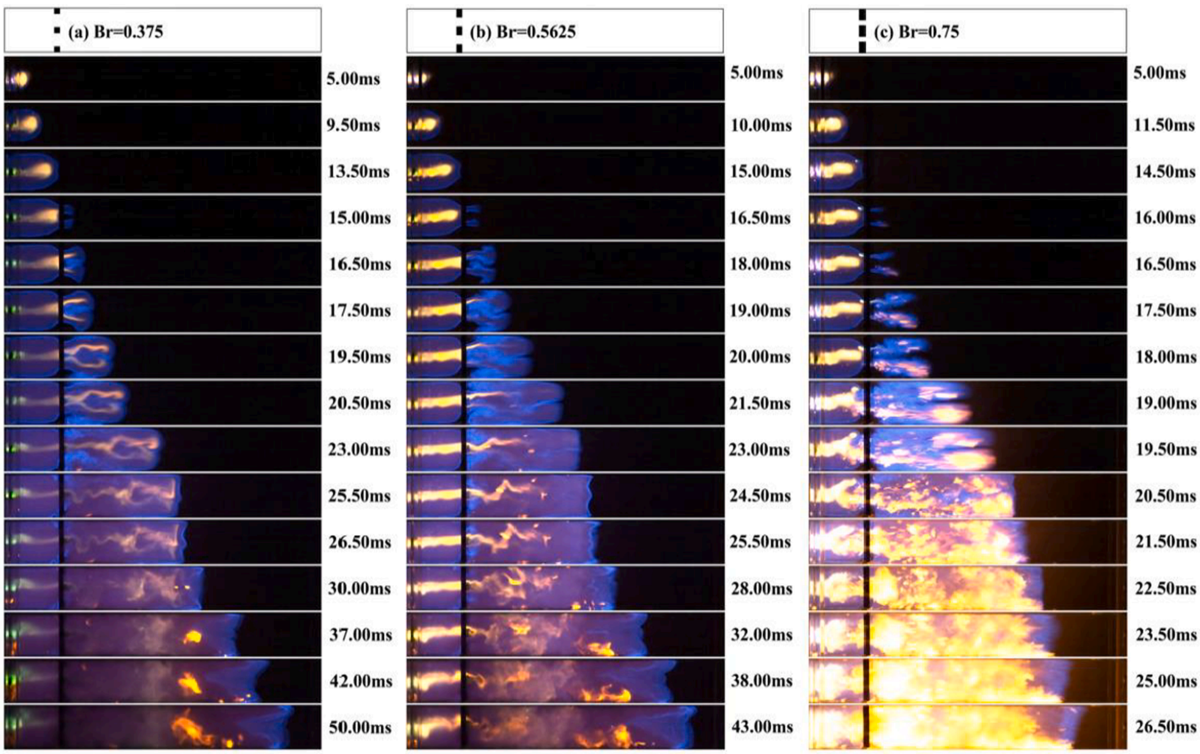

Fig. 5. Snapshot of the flame front at Position-1 with two-channel obstacle.

remain independent until the end of propagation as the two tulip flames collapse into one tulip shape.

In Fig. 5 (b), the flame is stretched by the shear layer [56] after passing through the two-channel obstacle. The flame jets behind the obstacle and the propagation direction remains horizontal (t = 16.5 ms). The reasons for this are that as Br increases, a longer shear layer can be formed to drive the flame out of the obstacle and maintain the divided. Interestingly, the split flames generate instability at different locations, with the top flame generating instability at the front and the bottom flame generating instability at the stem. Two parts of the flame erode each other due to KHI, and the fusion boundary is more turbulent (between t = 20 ms and t = 21.5 ms) compared to Fig. 5 (a). After the fusion, the flame still experiences the double tulip flame collapse into one.

As the Br increased again in Fig. 5 (c), the delayed combustion of the remaining fuel in the flame stem pushes the flame front development [43] when the flame jets out rapidly. As the split flame extends to the sides at the beginning stage, it causes the flame to prolong the fusion time. As the Br increases, the flame will propagate faster, and the double tulip flame fails to collapse into a full.

Fig. 6 shows the flame with the obstacle at Position-2. In Fig. 6 (a), the flame exhibits a more pronounced KHI after passing through the obstacle, and the flame becomes distorted (t = 26.5 ms). This accelerates the flame fusion process. Unlike before, irregular flame fronts are present throughout the split-fusion process. The increase in the RTI leads to an increase in the inward depression of the double tulip flame. The final flame collapses into a jagged tulip flame. When the Br = 0.5625, the flame "contests" the premixed gas. At the initiation of passing the obstacle, the free diffusion of one flame is bound to cause a squeeze on the other flame (see Fig. 6 (b), t = 25 ms). Interestingly, the flame fronts show two sharper fronts in the process of fusion. Both fronts maintain their independence in the subsequent propagation and do not completely fuse together until a complete tulip flame forms. In Fig. 6 (c), the flames fuse earlier and the split parts do not show a clear independent propagation process. However, the fused flame still has a stronger turbulence. The boundary of the flame front is not obvious and fails to form a clear double tulip structure, instead of a cellular flame [47].

Fig. 7 presents the flame as the obstacle at Position-3. The premixed gas is less disturbed in the early stage as the obstacle moves away from the ignition. In Fig. 7 (a), after the flame passes through the obstacles, the priority expansion at the flame front consumes the fuel. The flame that late to pass through the obstacle attached to the priority part

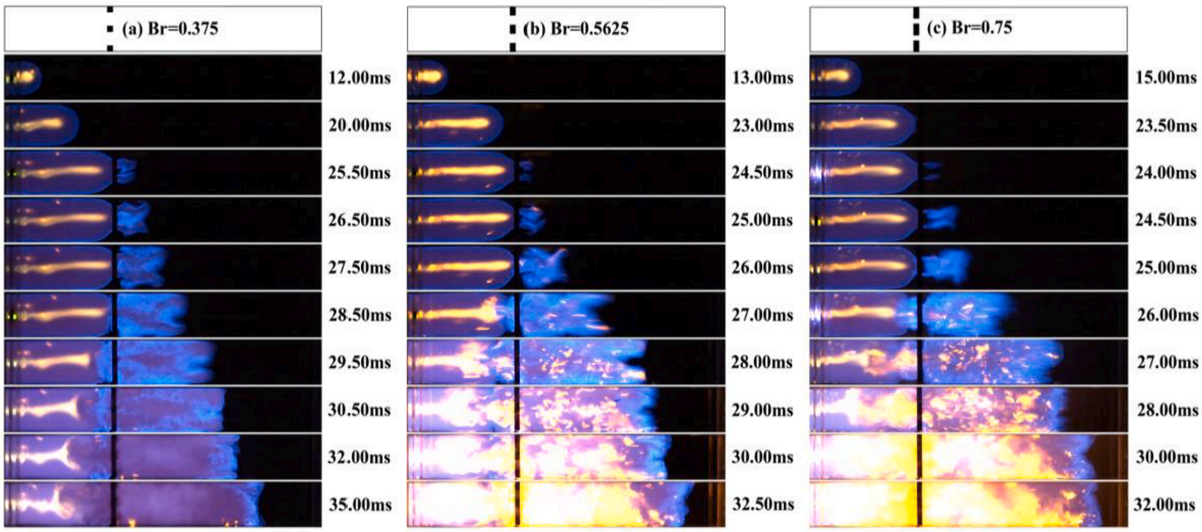

Fig. 6. Snapshot of the flame front at Position-2 with two-channel obstacle.

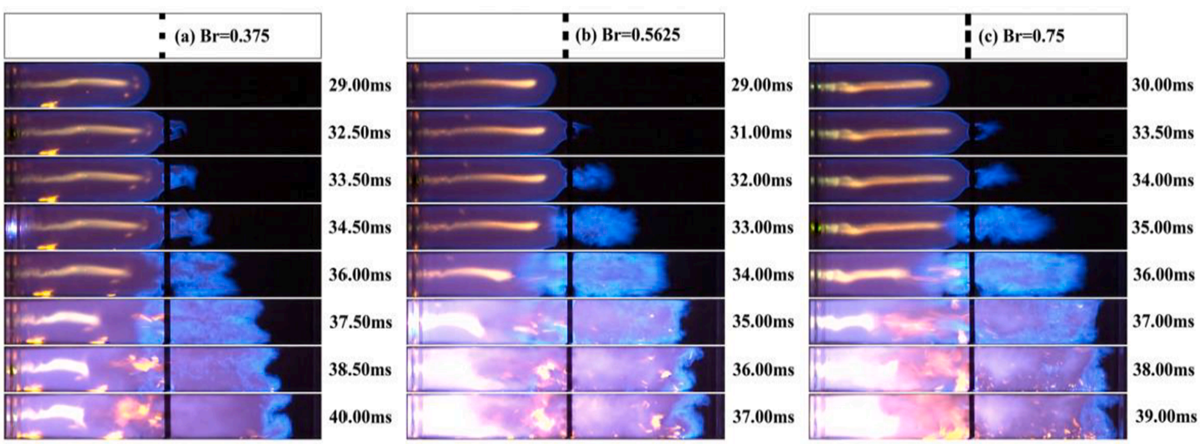

Fig. 7. Snapshot of the flame front at Position-3 two-channel obstacle.

(between t = 32.5 ms and t = 34.5 ms). In Fig. 7 (b), one flame front recoil and begins to wrap around the other divided flame due to multiple KHI. The flames begin to spread freely in all directions as they fuse and gradually form the major structure. In Fig. 7 (c) the flames fuse at the initial stage when passing the obstacle. The flames propagate with a main front and reverse at t = 37 ms. As the obstacle moved away from the ignition, the flames are more likely to fuse after passing through the two-channel obstacle. The reason is that the flame has less energy to maintain the split and quickly consumes the vortex.

3.2. *Flame split-fusion mechanism*

The flame boundary and propagation direction will change in the split-fusion process. Fig. 8 illustrates the details of the flame passing through the two-channel obstacle. As Br increases at Position-1, the more intense the flame split. The KHI is always accompanied by flame splitting. This induces turbulence at the intermediate boundary when the two split flames come into contact again and drives the flame development.

When the obstacle at Position-2, it is observed that the split flames compete for the premixed gas during the fusion process. The squeezing and erosion between the flames cause them to fuse. The irregular mixing and disordered turbulent combustion at the fusion boundary cause the propagation direction to change, and the longitudinal propagation of the flame front is greater than the transverse propagation. When the two-channel obstacle at Position-3, the vortex is consumed in an accelerated process that leads to preferential curling of the flame, and the flames eventually fuse together with the condition of losing the vortex hindrance that in the middle obstacle.

3.3. *Explosion flame front position and speed over time*

Fig. 9 shows the position of the flame front development with time. The diffusion of the flame in the spherical stage is not limited, and the position curve grows more rapidly. The positive feedback provided by the wall to the flame makes the flame position curve grow exponentially during the accumulation stage [11]. When the flame transforms into a tulip shape, the position curve shows linear growth.

When the obstacle is at Position-1, the flame front suddenly accelerates propagation after passing the obstacle causing the position curve to grow fast. Combined with Fig. 8, this is exactly the stage when the split flames fuse with each other, facilitating the propagation of the flame front. The influence on the initial flame is reduced by the increased distance of the obstacle from the ignition in Fig. 9 (c). The propagation of the flame front in the initial stage matches well. But the position curve still separates in the flame fusion stage depending on Br. In Fig. 9 (d), The flame front is affected by the precursor flow when it is close to a high barrier ratio obstacle that causing a slight drop in the

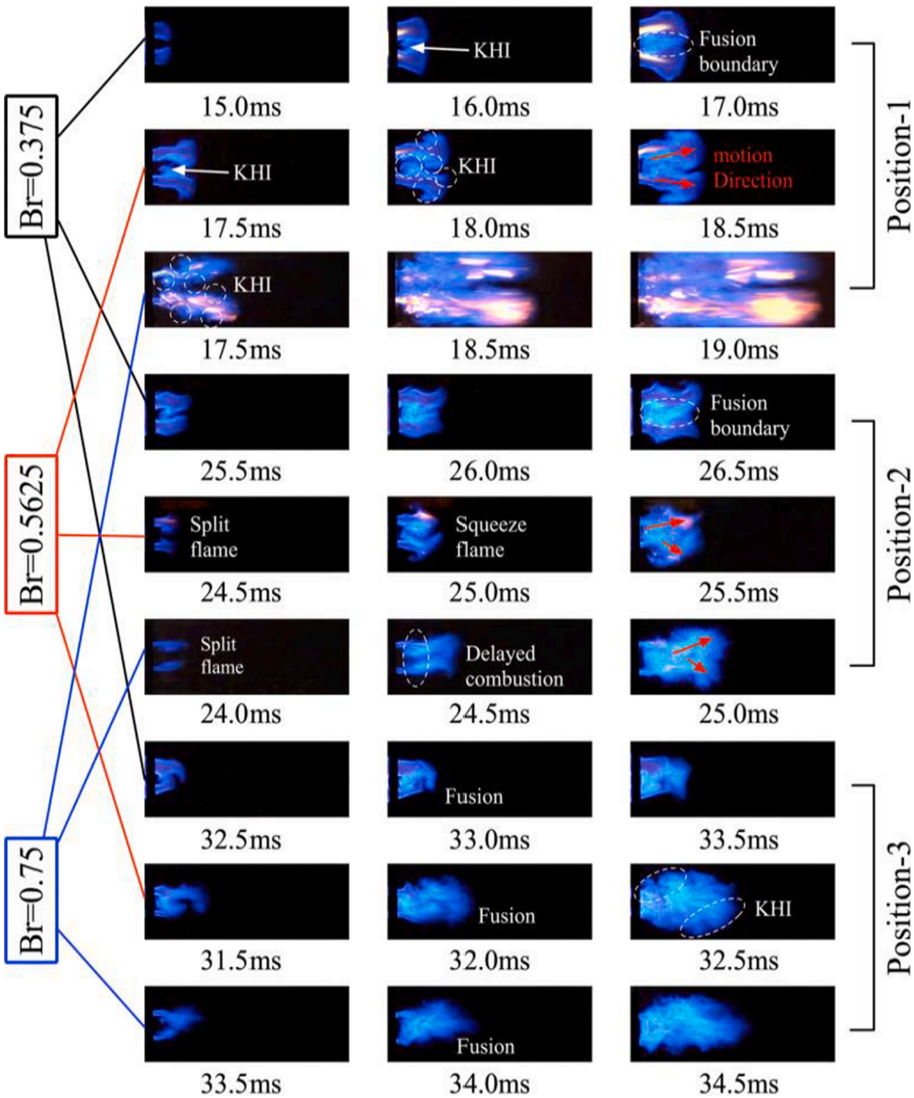

Fig. 8. Flame split and fusion details.

flame front [30]. However, the flame acceleration will compensate for the loss of position of the flame front. Therefore, the split and fusion of flames in the propagation process play a crucial role in the development of flames.

Flame speed is directly associated with flame structure variations [10]. Fig. 10 shows the relationship between flame speed and time. In Fig. 10 (a), the initial speed is relatively consistent with the no-obstacle case. After that, the flame propagation speed shows multiple peaks during the increase. The first acceleration of the flame front is due to the flame as it is extruded by the high-pressure zone at the edge of the two-channel obstacle. However, the initial flame expanding through the obstacle will cancel out this promotion effect, causing a brief drop in the lateral speed. The flame fusion and turbulence lead to a second acceleration. The maximum flame speed are 28.82 m/s, 44.28 m/s, and 92.21 m/s. The maximum flame speed increased by 76.05 %, 170.49 %, and 463.29 %. Thus, the increase in the barrier ratio will promote flame speed.

In Fig. 10 (b), the two-channel obstacle contributes most strongly to the flame speed. It is worth noting that the flame propagates through the complete finger-shaped stage possessing a certain initial speed. The flame turbulence caused by the obstacle plays a dominant role in promoting the speed and accelerating the process of splitting and fusion when the flame speed reaches its limiting maximum. The maximum flame speed are 52.0 m/s, 95.69 m/s, and 108.53 m/s, with Br increase, the maximum speed are increased by 217.65 %, 484.54 %, and 562.98 %, respectively. The promotion of the flame front is more sensitive to two-channel obstacles during the period of maximum speed development, and this also leads to the most efficient increase of flame front position (see Fig. 9 (c)).

However, the flame speed is less sensitive to the influence of the obstacle after the maximum period in Fig. 10 (c). There are three reasons for this phenomenon. The downstream position of the two-channel obstacle causes delayed turbulence transition. Meanwhile, the flame consumes the premixed fuel in the laminar combustion and reduces the support for turbulent flame acceleration. Another is the coupling relationship between the flame and pressure waves. The downstream movement of the obstacle compresses the space for flame acceleration, and the increase in reflected waves near the right wall counteracts the development of the flame. Finally, the increase in space pressure (see Fig. 11 (d)) causes the flame length to shorten and the flame to become thinner, which leads to a decrease in the flame front speed [57]. This also causes the flame front to increase only by a limited distance. The maximum values of flame speed are 52.15 m/s, 57.75 m/s, and 76.4 m/s as the Br increases. the increased are 218.57 %, 252.78 %, and 366.71

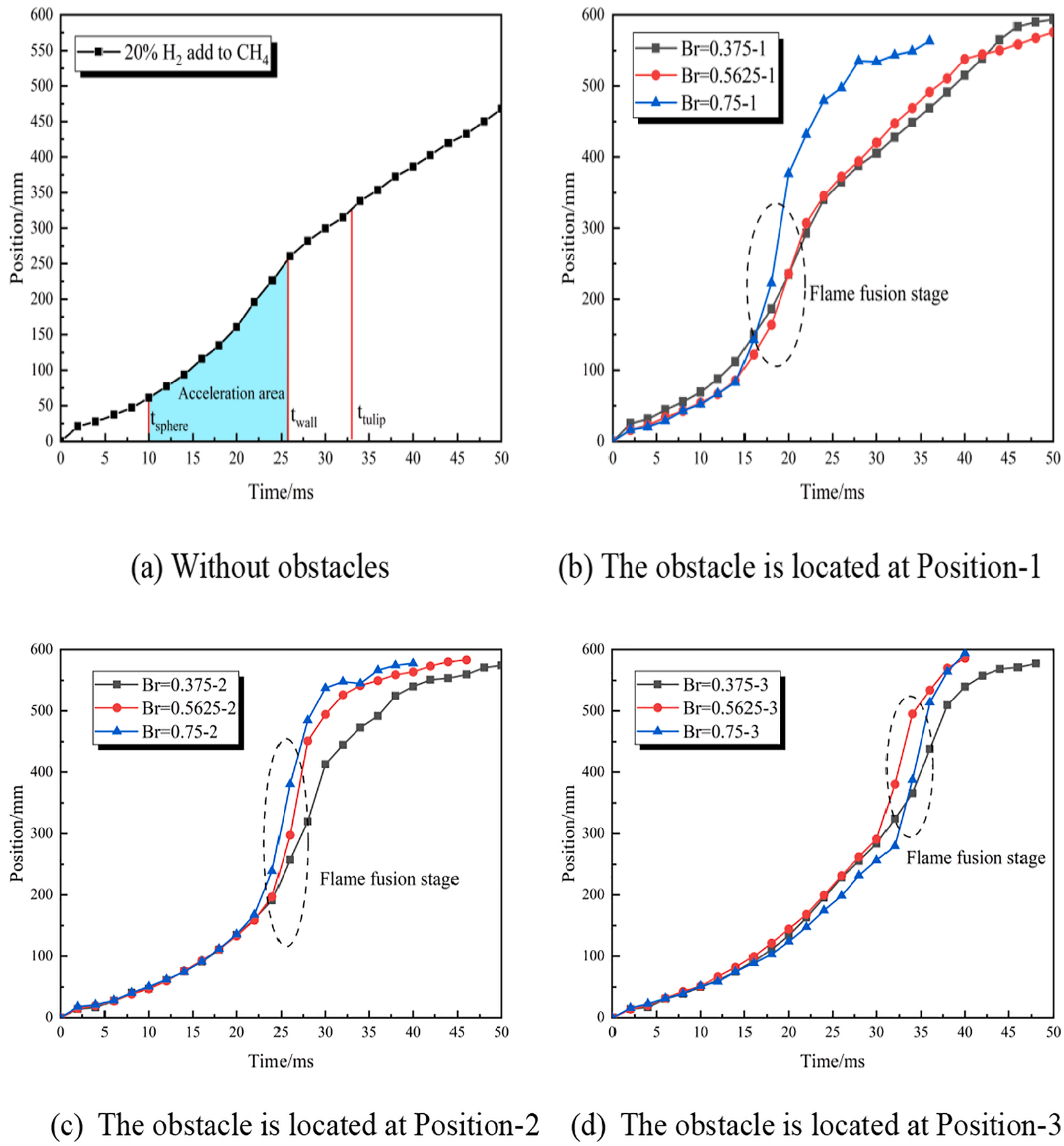

Fig. 9. Correspondence between the position of the flame front and time.

%. It can be concluded that the effect of obstacle position change on the maximum flame speed shows a tendency to increase and then decrease. An increase in the Br leads to an increase in the speed peak.

3.4. Explosion overpressure

Fig. 11 (a) indicates the explosion overpressure without the obstacle. There is a tight connection between flame structure and overpressure [58]. The overpressure exhibits an exponential growth trend during the spherical flame stage and the pre-finger shape stage. The overpressure curve exhibits Helmholtz oscillations and starts to decrease after reaching the maximum in the late-finger shape stage. There is only one peak in the overpressure during the propagation.

The effect of obstacles on the overpressure is shown in Fig. 11 (b) (c) (d). In Fig. 11 (b), The overpressure shifts from the original exponential to linear increase after passing through the obstacle. The pressure growth rate $\Delta P_S = 6.99$, $\Delta P_M = 13.25$, and $\Delta P_L = 55.42$ are obtained by linear fitting. The maximum pressure values are 66.0 kPa, 82.0 kPa, and 183.0 kPa. It is noteworthy that the process of flame structure transformation is advancing with the increase of Br. However, the accumulation trend of pressure corresponding to flame structure changes is nevertheless decreasing.

The increasing trend of overpressure in Fig. 11 (c) and (d) still changes from exponential to linear. The pressure growth rate is $\Delta P_s = 29.16$, $\Delta P_M = 48.48$, and $\Delta P_L = 70.78$ in Fig. 11 (c). The maximum pressure values are 125.0 kPa, 194.0 kPa, and 239.0 kPa. The pressure growth rate $\Delta P_S = 38.57$, $\Delta P_M = 74.27$, and $\Delta P_L = 75.28$ are obtained by fitting in Fig. 11 (d). The maximum pressure values are 147.0 kPa, 229.0 kPa, and 258.0 kPa. As the two-channel obstacle moves away from the ignition, the growth efficiency of overpressure in the linear growth period is increasing, and the local overpressure has a positive effect when the obstacle is far from the ignition. The space is continuously compressed during the downstream movement of the obstacle, and the pressure generated by the flame fusion process and the release of local pressure make the difference between the accumulation and release effectiveness of the downstream overpressure in increasing. Meanwhile, the pressure generated by the flame fusion serves as an auxiliary facilitator at this stage. They jointly lead to an increase in overpressure with the downstream movement of the obstacle. As the obstacle moves away from the ignition, the change with Br to the overpressure is gradually reduced. It is seen that in the early stages, the Br plays a major role in the increase of pressure. As the distance between the obstacle and the

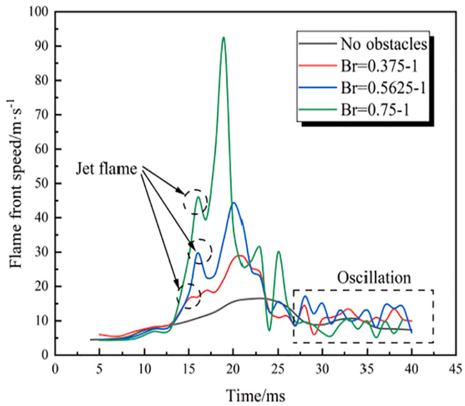

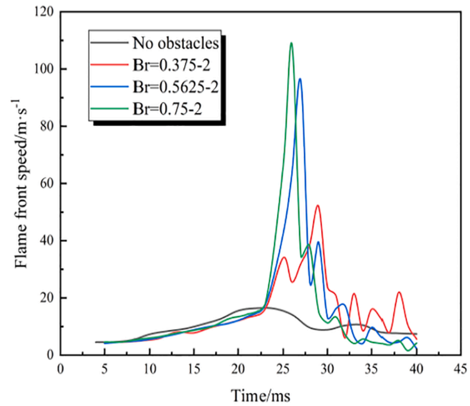

(a) Effect of obstacle at Position-1 on flame speed (b) Effect of obstacle at Position-2 on flame speed

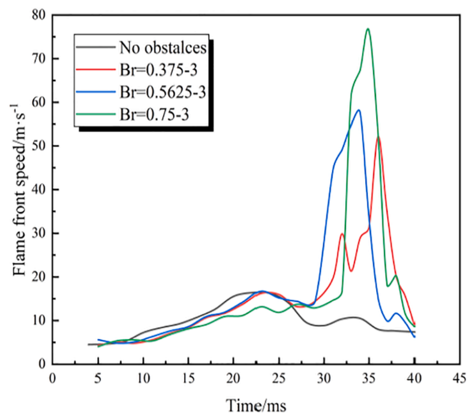

(c) Effect of obstacle at Position-3 on flame speed

Fig. 10. The relationship between flame front speed and time.

ignition increases, the overpressure difference caused by the two-channel obstacle decreases when the Br is more than about 50 %.

4. Numerical simulation results and discussions

4.1. Flame evolution process

The Position-1 case is used to illustrate the flame propagation, and the simulation flame is shown in Fig. 12. The simulation results and the experimental flame shooting are satisfied, the simulated flame fronts all demonstrate the phenomena generated in the experiment, verifying the validity of the RNG k-ε turbulence model in combination with the EDC model. First, the flame generates split after passing through the obstacle. Moreover, the flames fuse together in the subsequent propagation. When the flame fusion is completed, a double tulip structure, like in the experiment appears, which also collapses into a complete tulip shape over time. In the above discussion, it is shown that the tulip flame represents the instability exhibited by the flame. The split-fusion behavior of the flame resulting in a rapid increase in flame instability, and the split flame fronts all exhibit the tulip structure. However, as the flame proceeds to the terminal stage, the flame speed, and acceleration decrease, leading to the decay of the RTI at the flame boundary. Therefore, the process of double tulip flame collapse can also be considered a process of decaying due to the effect of flame instability, and the flame eventually progresses toward a stabilized state.

4.2. Vortex in the flow field

The tangents of the velocity vector constitute the streamlines, and the development pattern of the streamlines plays a crucial role in flame propagation. Fig. 13 illustrates the development of the vector streamlines during flame propagation.

When the Br = 0.375, vortices are formed behind the obstacle (downstream of flame propagation) and two symmetrical vortices are formed at the middle obstacle. The influence of the vortices gradually expands as the flame develops. The vortices are stretched longer as the flame passes through the obstacle. However, it is of interest that when the flame is split, the vortices behind the obstacle at both ends expand, but the vortices at the middle obstacle gradually become smaller until they disappear. This trend of the vortices action illustrates the reason why the flames converge and fuse toward the center. When the Br = 0.5625, the difference between the vortex at the two ends of the obstacle and the middle obstacle increases. The vortex at both ends shows a tendency of gradual expansion while the vortices at the middle obstacle are increasing and then decreasing in the development process. When the Br = 0.75, the vortices gradually expand after formation, and have a broader range. When the flame passes the obstacles, the vortex behind the obstacles at both ends creates a breakdown, from the initial one decomposes into two, and the vortex at the middle obstacle still gradually shrinks until it disappears. This more reasonably explains that the flame front exhibits multiple instabilities after passing through the two-channel obstacles at Br = 0.75. The outer edges of two-channel obstacles closer to the wall are more likely to shed larger vortices that stretch and change the flame shape. The inner edge near the center tends to shed

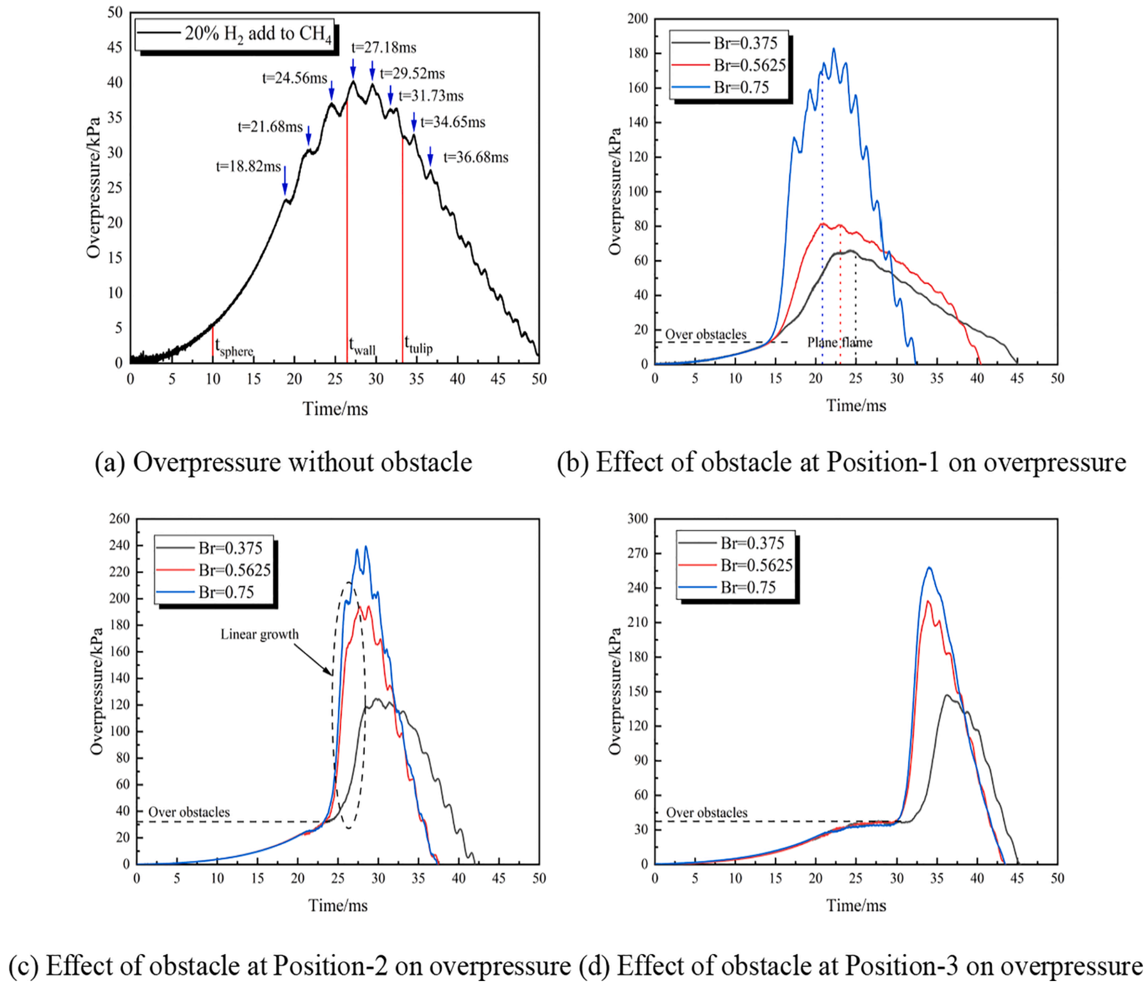

Fig. 11. Variation of explosion overpressure with time.

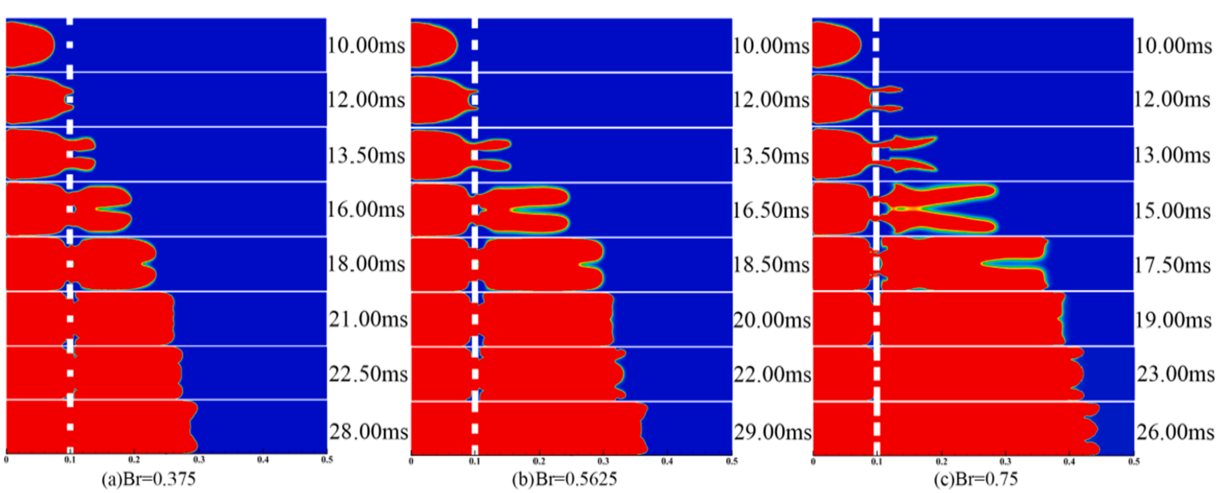

Fig. 12. Simulation flame propagation process.

smaller vortices that disturb the flame boundary, forcing the flames to converge toward the center and thus fusion occurs.

Fig. 14 presents the distribution of the vorticity, and the intensity of vortices can be observed through the vorticity [59]. The vorticity criterion $\Omega = \partial u_y/\partial x - \partial u_x/\partial y$. The analysis reveals that the vorticity with the counterclockwise flow is positive and the vorticity with the clockwise flow is negative. Whereas the vorticity originates from the change in velocity gradient due to the obstacle [60], the flame does not exhibit the vorticity change until it passes through the obstacle region. As the Br increases, the vorticity affects a greater range and intensity. This also illustrates that the Br increases, the longer the shear layer formed behind the obstacle.

When the flame passes through the obstacles, the vorticity concentrates more at the boundary of the flame front, and the vorticity at the

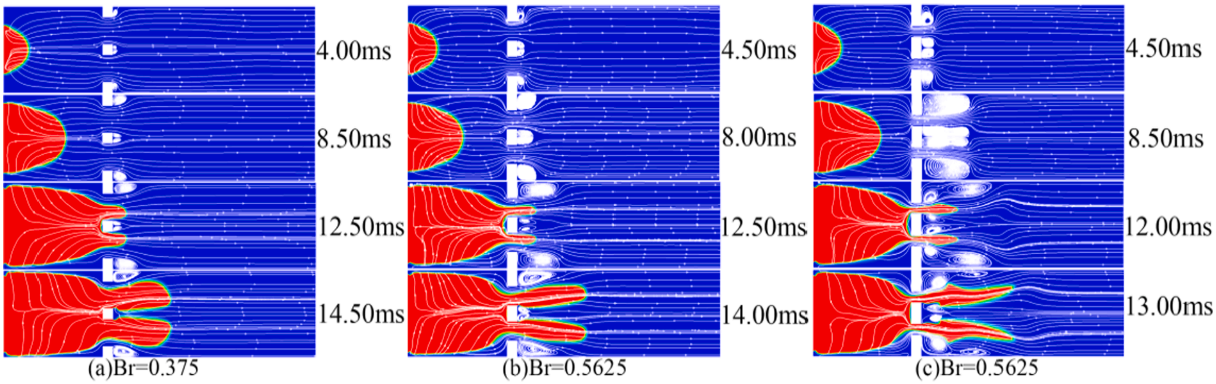

Fig. 13. The law of streamlines development.

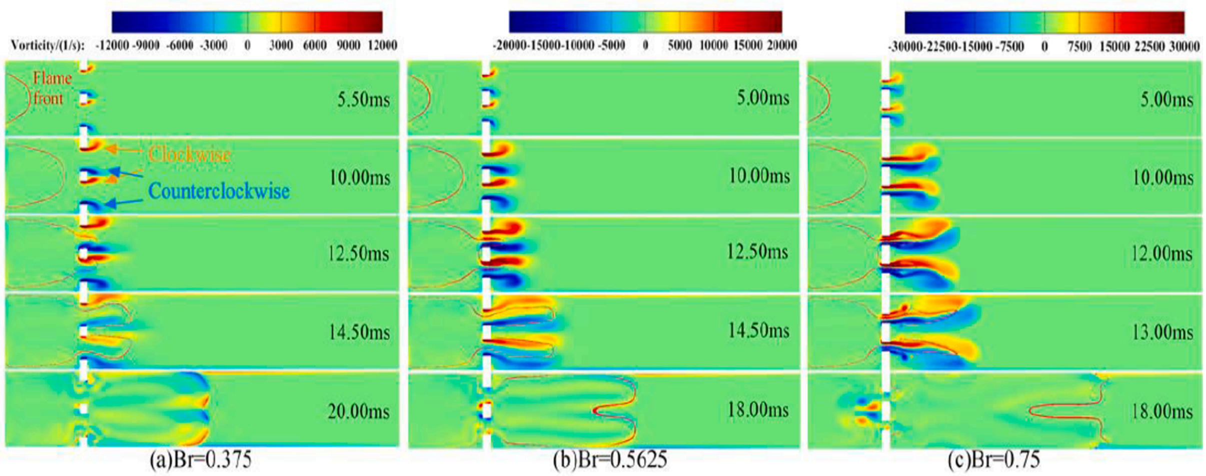

Fig. 14. Vorticity field distribution.

obstacles gradually disappears currently. The reason for the analysis is that after the flame passes through the obstacle, the turbulence of the flame increases, and the reaction of the flame boundary with the premixed fuel increases and shows a chaotic flow. This pattern leads to the chaotic direction of the shear force acting on the combustion production. Therefore, the vorticity is mainly visible at the flame boundary.

Two vortices in opposite directions are formed at every-two edges of the middle obstacle, which offset each other and gradually dissipate. For Br = 0.75, the formation of multiple vorticities is the result of the old vortices not completely dissipating and new vortices forming again.

4.3. Flame turbulence intensity

The turbulent kinetic energy (TKE) enables measuring the turbulent intensity of the explosion reaction [61]. In Fig. 15, The TKE at the flame boundary and the obstacle edge is greater during the flame front propagation. The TKE is first enhanced by the chemical reaction at the flame boundary and the strong flow at the obstacle boundary. When the flame fusion, the turbulence intensity in the fusion region is significantly greater than others. This illustrates the mechanism of flame fusion acceleration, where the stronger TKE can enhance the flame to accelerate. As the Br increases, In Fig. 15 (c), the turbulence intensity can increase

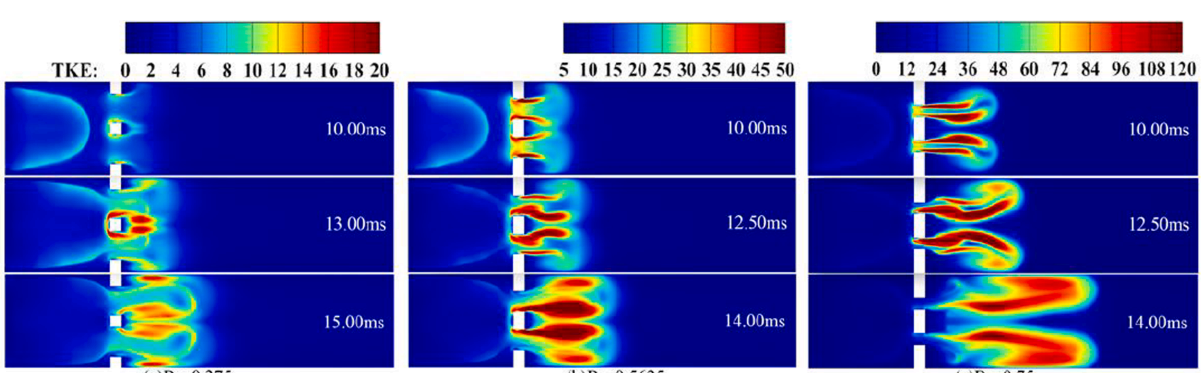

Fig. 15. Turbulence intensity characteristics.

again when the flame stem tends to fuse, promoting the flame development.

5. Conclusions

The effect of obstacle barrier ratio and position on the premixed flame is investigated in experimental and numerical simulation. The main conclusions are as follows:

(1) Variations in the position of the two-channel obstacle can lead to diverse split-fusion processes. Flame morphology becomes confused as the two-channel obstacle away from the ignition, and the flames tend to fuse. The increase in the two-channel Br will elongate the shear layer, while the Kelvin-Helmholtz instability in multiple regions makes the split flame more turbulent.
(2) The maximum flame speed increases and then decreases as the two-channel obstacle moves away from the ignition. The two-channel obstacle at the location of the original maximum flame propagation speed contributes most strongly to the flame speed. The maximum speed of the flame can be increased by more than 5 times, and the flame front acceleration propagation distance is increased.
(3) The flame splitting causes an increase in the accumulation of local pressure. The maximum pressure monotonically increases and exceeds 6 times as the obstacle away from the ignition.
(4) The expansion and dissipation of the vortex behind the obstacle drive the flame to fusion. The vortex behind the middle obstacle tends to dissipate due to the simultaneous positive and negative vorticity fields. During the flame fusion, the turbulence intensity at the flame boundary is greater, and the two enhance each other's development.

CRediT authorship contribution statement

Shuo Wang: Methodology, Software, Validation, Data curation, Writing – original draft, Writing – review & editing. **Guoqing Xiao:** Conceptualization, Resources, Writing – review & editing, Supervision, Funding acquisition. **Hongfu Mi:** Resources, Writing – review & editing, Supervision, Project administration, Funding acquisition. **Yu Feng:** Software, Resources, Writing – review & editing. **Jian Chen:** Visualization, Supervision.

Declaration of Competing Interest

The authors declare that they have no known competing financial interests or personal relationships that could have appeared to influence the work reported in this paper.

Data availability

No data was used for the research described in the article.

Acknowledgements

This work is supported by National Natural Science Foundation of China (51874255, 52174209, 52274177), Chongqing Key Laboratory of Fire and Explosion Safety (LQ21KFJJ08). The authors are grateful for the numerical simulation support from the Computational Biofluidics and Biomechanics Laboratory (CBBL) at Oklahoma State University, USA.

References

[1] Gillessen B, Heinrichs H, Hake J-F, Allelein H-J. Natural gas as a bridge to sustainability: Infrastructure expansion regarding energy security and system transition. Appl Energy 2019;251:113377. https://doi.org/10.1016/j.apenergy.2019.113377.
[2] Lin B, Li Z. Towards world's low carbon development: the role of clean energy. Appl Energy 2022;307:118160. https://doi.org/10.1016/j.apenergy.2021.118160.
[3] Chen Z, Dai P, Chen S. A model for the laminar flame speed of binary fuel blends and its application to methane/hydrogen mixtures. Int J Hydrogen Energy 2012;37:10390–6. https://doi.org/10.1016/j.ijhydene.2012.04.015.
[4] Klell M, Eichlseder H, Sartory M. Mixtures of hydrogen and methane in the internal combustion engine-Synergies, potential and regulations. Int J Hydrogen Energy 2012;37:11531–40. https://doi.org/10.1016/j.ijhydene.2012.03.067.
[5] Halter F, Chauveau C, Gökalp I. Characterization of the effects of hydrogen addition in premixed methane/air flames. Int J Hydrogen Energy 2007;32:2585–92. https://doi.org/10.1016/j.ijhydene.2006.11.033.
[6] Khan I, Zakari A, Zhang J, Dagar V, Singh S. A study of trilemma energy balance, clean energy transitions, and economic expansion in the midst of environmental sustainability: New insights from three trilemma leadership. Energy 2022:123619. 10.1016/j.energy.2022.123619.
[7] Yin W, Fu G, Yang C, Jiang Z, Zhu K, Gao Y. Fatal gas explosion accidents on Chinese coal mines and the characteristics of unsafe behaviors: 2000–2014. Saf Sci 2017;92:173–9. https://doi.org/10.1016/j.ssci.2016.09.018.
[8] Chen H, Qi H, Feng Q. Characteristics of direct causes and human factors in major gas explosion accidents in Chinese coal mines: case study spanning the years 1980–2010. J Loss Prev Process Ind 2013;26:38–44. https://doi.org/10.1016/j.jlp.2012.09.001.
[9] Zheng K, Yu M, Zheng L, Wen X, Chu T, Wang L. Experimental study on premixed flame propagation of hydrogen/methane/air deflagration in closed ducts. Int J Hydrogen Energy 2017;42:5426–38. https://doi.org/10.1016/j.ijhydene.2016.10.106.
[10] Xiao H, Duan Q, Sun J. Premixed flame propagation in hydrogen explosions. Renew Sustain Energy Rev 2018;81:1988–2001. https://doi.org/10.1016/j.rser.2017.06.008.
[11] Bychkov V, Akkerman V, Fru G, Petchenko A, Eriksson L-E. Flame acceleration in the early stages of burning in tubes. Combust Flame 2007;150:263–76. https://doi.org/10.1016/j.combustflame.2007.01.004.
[12] Kasmani RM, Andrews GE, Phylaktou HN. Experimental study on vented gas explosion in a cylindrical vessel with a vent duct. Process Saf Environ Prot 2013;91:245–52. https://doi.org/10.1016/j.psep.2012.05.006.
[13] Hall R, Masri AR, Yaroshchyk P, Ibrahim SS. Effects of position and frequency of obstacles on turbulent premixed propagating flames. Combust Flame 2009;156:439–46. https://doi.org/10.1016/j.combustflame.2008.08.002.
[14] Ciccarelli G, Dorofeev S. Flame acceleration and transition to detonation in ducts. Prog Energy Combust Sci 2008;34:499–550. https://doi.org/10.1016/j.pecs.2007.11.002.
[15] Xiao H, Houim RW, Oran ES. Formation and evolution of distorted tulip flames. Combust Flame 2015;162:4084–101. https://doi.org/10.1016/j.combustflame.2015.08.020.
[16] Dunn-Rankin D, Sawyer RF. Tulip flames: Changes in shape of premixed flames propagating in closed tubes. Exp Fluids 1998;24:130–40. https://doi.org/10.1007/s003480050160.
[17] Cao X, Wei H, Wang Z, Wang Y, Fan L, Lu Y. Effect of obstacle on the H2/CO/Air explosion characteristics under lean-fuel conditions. Fuel 2022;319:123834. https://doi.org/10.1016/j.fuel.2022.123834.
[18] Zhang B, Li Z, Xia Y, Shi J, Zhang J, Wang B, et al. Experimental study on the combined effects of obstacles and local water mist on gas explosion for maritime safety. International Journal of Naval Architecture and Ocean Engineering 2021:100424. doi: 10.1016/j.ijnaoe.2021.11.007.
[19] Li Y, Bi M, Zhou Y, Jiang H, Huang L, Zhang K, et al. Experimental and theoretical evaluation of hydrogen cloud explosion with built-in obstacles. Int J Hydrogen Energy 2020;45:28007–18. https://doi.org/10.1016/j.ijhydene.2020.07.067.
[20] Yang X, Yu M, Zheng K, Luan P, Han S. An experimental study on premixed syngas/air flame propagating across an obstacle in closed duct. Fuel 2020;267:117200. https://doi.org/10.1016/j.fuel.2020.117200.
[21] Zheng K, Song C, Yang X, Wu J, Jiang J, Xing Z. Effect of obstacle location on explosion dynamics of premixed H2/CO/air mixtures in a closed duct. Fuel 2022;324:124703. https://doi.org/10.1016/j.fuel.2022.124703.
[22] Zhang K, Wang Z, Ni L, Cui Y, Zhen Y, Cui Y. Effect of one obstacle on methane–air explosion in linked vessels. Process Saf Environ Prot 2017;105:217–23. https://doi.org/10.1016/j.psep.2016.11.004.
[23] Li H, Guo J, Tang Z, Li J, Huang P, Zhang S. Effects of ignition, obstacle, and side vent locations on vented hydrogen–air explosions in an obstructed duct. Int J Hydrogen Energy 2019;44:20598–605. https://doi.org/10.1016/j.ijhydene.2019.06.029.
[24] Zhou Y, Li Y, Jiang H, Zhang K, Chen X, Huang L, et al. Investigations on unconfined large-scale methane explosion with the effects of scale and obstacles. Process Saf Environ Prot 2021;155:1–10. https://doi.org/10.1016/j.psep.2021.09.004.
[25] Wen X, Yu M, Ji W, Yue M, Chen J. Methane-air explosion characteristics with different obstacle configurations. Int J Min Sci Technol 2015;25:213–8. https://doi.org/10.1016/j.ijmst.2015.02.008.
[26] Lv X, Zheng L, Zhang Y, Yu M, Su Y. Combined effects of obstacle position and equivalence ratio on overpressure of premixed hydrogen–air explosion. Int J Hydrogen Energy 2016;41:17740–9. https://doi.org/10.1016/j.ijhydene.2016.07.263.
[27] Schiavetti M, Carcassi MN. Experimental tests of inhomogeneous hydrogen deflagrations in the presence of obstacles. Int J Hydrogen Energy 2021;46:12455–63. https://doi.org/10.1016/j.ijhydene.2020.09.100.

[28] Henriksen M, Vaagsaether K, Lundberg J, Forseth S, Bjerketvedt D. Simulation of a premixed explosion of gas vented during Li-ion battery failure. Fire Saf J 2021;126: 103478. https://doi.org/10.1016/j.firesaf.2021.103478.

[29] Gao K, Li S, Liu Y, Jia J, Wang X. Effect of flexible obstacles on gas explosion characteristic in underground coal mine. Process Saf Environ Prot 2021;149:362–9. https://doi.org/10.1016/j.psep.2020.11.004.

[30] Gamezo VN, Bachman CL, Oran ES. Flame acceleration and DDT in large-scale obstructed channels filled with methane-air mixtures. Proc Combust Inst 2021;38: 3521–8. https://doi.org/10.1016/j.proci.2020.09.018.

[31] Qin Y, Chen X. Study on the dynamic process of in-duct hydrogen-air explosion flame propagation under different blocking rates. Int J Hydrogen Energy 2022. https://doi.org/10.1016/j.ijhydene.2022.04.004.

[32] di Sarli V, di Benedetto A, Russo G. Large Eddy Simulation of transient premixed flame–vortex interactions in gas explosions. Chem Eng Sci 2012;71:539–51. https://doi.org/10.1016/j.ces.2011.11.034.

[33] Xing H, Qiu Y, Sun S, Wang M, Li B, Xie L. Experimental study of overpressure and temperature field behaviors of a methane-air mixture with different ignition positions, solid structure obstacles and initial turbulence levels. Fuel 2021;287: 119446. https://doi.org/10.1016/j.fuel.2020.119446.

[34] Qin Y, Chen X. Flame propagation of premixed hydrogen-air explosion in a closed duct with obstacles. Int J Hydrogen Energy 2021;46:2684–701. https://doi.org/10.1016/j.ijhydene.2020.10.097.

[35] Xiao G, Wang S, Mi H, Khan F. Analysis of obstacle shape on gas explosion characteristics. Process Saf Environ Prot 2022;161:78–87. https://doi.org/10.1016/j.psep.2022.03.019.

[36] Hariharan A, Wichman IS. Premixed flame propagation and morphology in a constant volume combustion chamber. Combust Sci Technol 2014;186:1025–40. https://doi.org/10.1080/00102202.2014.897340.

[37] Zheng K, Wu Q, Chen C, Xing Z, Hao Y, Yu M. Explosion behavior of non-uniform methane/air mixture in an obstructed duct with different blockage ratios. Energy 2022;255:124603. https://doi.org/10.1016/j.energy.2022.124603.

[38] Xiao H, Wang Q, He X, Sun J, Shen X. Experimental study on the behaviors and shape changes of premixed hydrogen-air flames propagating in horizontal duct. Int J Hydrogen Energy 2011;36:6325–36. https://doi.org/10.1016/j.ijhydene.2011.02.049.

[39] Wen X, Wang M, Su T, Zhang S, Pan R, Ji W. Suppression effects of ultrafine water mist on hydrogen/methane mixture explosion in an obstructed chamber. Int J Hydrogen Energy 2019;44:32332–42. https://doi.org/10.1016/j.ijhydene.2019.10.110.

[40] Duan Y, Long F, Huang J, Jia H, Bu Y, Yu S. Effects of porous materials with different thickness and obstacle layout on methane/hydrogen mixture explosion with low hydrogen ratio. Int J Hydrogen Energy 2022;47:27237–49. https://doi.org/10.1016/j.ijhydene.2022.06.065.

[41] Isaac T. HyDeploy: The UK's First Hydrogen Blending Deployment Project. Clean Energy 2019;3:114–25. https://doi.org/10.1093/ce/zkz006.

[42] Yu M, Luan P, Zheng K, Yang X, Han S, Duan Y. Experimental study on explosion characteristics of syngas with different ignition positions and hydrogen fraction. Int J Hydrogen Energy 2019;44:15553–64. https://doi.org/10.1016/j.ijhydene.2019.04.046.

[43] Han S, Yu M, Yang X, Wang X. Effects of obstacle position and hydrogen volume fraction on premixed syngas-air flame acceleration. Int J Hydrogen Energy 2020; 45:29518–32. https://doi.org/10.1016/j.ijhydene.2020.07.189.

[44] Zhou G, Kong Y, Qian X, Zhang Q, Ma Y, Wu D. Explosion dynamics and sensitivity analysis of blended LPG/DME clean fuel promoted by H2 in a confined elongated space. Fuel 2023;331:125816. https://doi.org/10.1016/j.fuel.2022.125816.

[45] Song Y, Zhang Y, Chen Y, Liu X, Fu M, Li Y. Numerical investigation of effects on premixed hydrogen/air flame propagation in pipes with different contraction or expansion angles. J Loss Prev Process Ind 2021;70:104201. https://doi.org/10.1016/j.jlp.2020.104201.

[46] Nguyen T, Strebinger C, Bogin GE, Brune J. A 2D CFD model investigation of the impact of obstacles and turbulence model on methane flame propagation. Process Saf Environ Prot 2021;146:95–107. https://doi.org/10.1016/j.psep.2020.08.023.

[47] Zheng K, Yu M, Liang Y, Zheng L, Wen X. Large eddy simulation of premixed hydrogen/methane/air flame propagation in a closed duct. Int J Hydrogen Energy 2018;43:3871–84. https://doi.org/10.1016/j.ijhydene.2018.01.045.

[48] Qi B, Deng H, Yu M, Li H, Yang X. Numerical investigation on the effects of reaction orders on the flame propagation dynamic behaviors for premixed gas in a closed tube. Int J Hydrogen Energy 2022;47:8037–47. https://doi.org/10.1016/j.ijhydene.2021.12.096.

[49] Deng H, Huang M, Wen X, Chen G, Wang F, Yao Z. Numerical investigation of premixed methane-air flame in two-dimensional half open tube in the early stages. Fuel 2020;272:117709. https://doi.org/10.1016/j.fuel.2020.117709.

[50] Xiao H, Sun J, He X. A study on the dynamic behavior of premixed propane-air flames propagating in a curved combustion chamber. Fuel 2018;228:342–8. https://doi.org/10.1016/j.fuel.2018.04.165.

[51] Gran IR, Magnussen BF. A numerical study of a bluff-body stabilized diffusion flame. Part 2. Influence of combustion modeling and finite-rate chemistry. Combust Sci Technol 1996;119:191–217. https://doi.org/10.1080/00102209608951999.

[52] Xiao H, He X, Duan Q, Luo X, Sun J. An investigation of premixed flame propagation in a closed combustion duct with a 90° bend. Appl Energy 2014;134: 248–56. https://doi.org/10.1016/j.apenergy.2014.07.071.

[53] Clanet C, Searby G. On the "Tulip flame" phenomenon. Combust Flame 1996;105: 225–38. https://doi.org/10.1016/0010-2180(95)00195-6.

[54] Xiao H, An W, Duan Q, Sun J. Dynamics of premixed hydrogen/air flame in a closed combustion vessel. Int J Hydrogen Energy 2013;38:12856–64. https://doi.org/10.1016/j.ijhydene.2013.07.082.

[55] Xiao H, Wang Q, Shen X, Guo S, Sun J. An experimental study of distorted tulip flame formation in a closed duct. Combust Flame 2013;160:1725–8. https://doi.org/10.1016/j.combustflame.2013.03.011.

[56] Li Q, Sun X, Wang X, Zhang Z, Lu S, Wang C. Experimental study of flame propagation across flexible obstacles in a square cross-section channel. Int J Hydrogen Energy 2019;44:3944–52. https://doi.org/10.1016/j.ijhydene.2018.12.085.

[57] Ziani L, Chaker A. Ambient pressure effect on non-premixed turbulent combustion of CH4–H2 mixture. Int J Hydrogen Energy 2016;41:11842–7. https://doi.org/10.1016/j.ijhydene.2015.11.167.

[58] Xiao H, Houim RW, Oran ES. Effects of pressure waves on the stability of flames propagating in tubes. Proceedings of the Combustion Institute 2017;36:1577–83. doi: 10.1016/j.proci.2016.06.126.

[59] Shanbhogue SJ, Plaks D V., Lieuwen T. The K-H instability of reacting, acoustically excited bluff-body shear layers. Collection of Technical Papers - 43rd AIAA/ASME/SAE/ASEE Joint Propulsion Conference, vol. 7, American Institute of Aeronautics and Astronautics; 2007, p. 6631–47. doi: 10.2514/6.2007-5680.

[60] Lei J, Liu N, Jiao Y, Zhang S. Experimental investigation on flame patterns of buoyant diffusion flame in a large range of imposed circulations. Proceedings of the Combustion Institute 2017;36:3149–56. doi: 10.1016/j.proci.2016.06.072.

[61] Jiang H, Bi M, Gao Z, Zhang Z, Gao W. Effect of turbulence intensity on flame propagation and extinction limits of methane/coal dust explosions. Energy 2022; 239:122246. https://doi.org/10.1016/j.energy.2021.122246.